A&A 375, 539–552 (2001)
DOI: 10.1051/0004-6361:20010654

Astronomy & Astrophysics

Near-infrared imaging of compact HII regions in Cygnus X⋆,⋆⋆

F. Comerón[1] and J. Torra[2]

[1] European Southern Observatory, Karl-Schwarzschild-Str. 2, 85748 Garching bei München, Germany
[2] Departament d'Astronomia i Meteorologia, Universitat de Barcelona, Av. Diagonal 647, 08028 Barcelona, Spain
e-mail: jordi@am.ub.es

Received 24 January 2001 / Accepted 12 April 2001

Abstract. We present a near-infrared imaging survey of compact HII regions in the direction of the Cygnus X complex, for which no previous observations at those wavelengths have been published so far. The targets have been selected from a catalog of sources in that region having a thermal spectral energy distribution between 408 and 4800 MHz (Wendker et al. 1991), and an inferred angular size smaller than 5 arcmin across. We present images in the JHK filters, color-magnitude, and color-color diagrams for each region. We also suggest and apply a method for estimating the distance by comparing the dereddened H-band flux from all the stars in the area of the HII region and the radio-continuum flux. Many of the regions imaged are clearly associated with stellar aggregates with different degrees of concentration, whose components show varying amounts of extinction. Some objects are often found in the region of the $(J-H)$, $(H-K)$ diagram indicating excess emission of circumstellar nature. A detailed discussion on each object is provided in the context of existing published observations at different wavelengths, in particular regarding the existence of ultracompact components. A number of ultracompact HII regions are found to have clearly visible unresolved or nearly unresolved K-band counterparts characterized by very red $H-K$ colors, suggesting that the extinction may be low enough in their direction so as to allow the direct observation of the star ionizing the ultracompact component.

Key words. stars: early-type – HII regions – Cygnus X

1. Introduction

The Cygnus X complex of molecular clouds (Bolton & Westford 1950; Piddington & Minnett 1952) stands out as one of the richest aggregates of star forming regions in our galactic neighborhood. It appears projected in an area of the sky containing many other structures related to massive star formation and violent processes in the interstellar medium (Bochkarev & Sitnik 1985). The inventory includes the OB associations of the Cygnus arm (including the massive association Cygnus OB2; e.g. Knödlseder 2000 and references therein), the X-ray emitting Cygnus Superbubble, and several other star forming regions revealed by IRAS (Odenwald & Schwartz 1993). A vast amount of observations of Cygnus X, mostly at radio, far, and mid-infrared wavelengths (e.g. Dobashi et al. 1996), have produced comprehensive pictures at various resolution scales of the different individual components of the complex, as well as of its large scale structure. Numerous individual HII regions, first noted by Downes & Rinehart (1968), as well as young supernova remnants, have been revealed in these studies.

The many individual compact HII regions of Cygnus X have important potential for the study of the three-dimensional structure of the complex and its present star-forming activity. They also make up an appropriate sample showing the variety of morphologies that can arise from the interaction of small- and medium-sized aggregates of massive stars with the interstellar medium, while the fact that many of them may be physically related to a single, large complex allows one to study them at a similar spatial resolution using a single instrumental setup. Besides providing flux-limited complete samples of compact HII regions in Cygnus X, observations published to date at radio wavelengths have yielded insights on the morphological and kinematical properties of the ionized gas, while IRAS observations in the mid-infrared (Odenwald 1989; Odenwald & Schwartz 1993) have allowed the

Send offprint requests to: F. Comerón,
e-mail: fcomeron@eso.org

⋆ Based on observations collected at the Observatorio del Teide (Tenerife, Spain).

⋆⋆ The complete Fig. 1 is available in electronic form at http://www.edpsciences.org and Table 2 is only available in electronic form at the CDS via anonymous ftp to cdsarc.u-strasbg.fr (130.79.128.5) or via http://cdsweb.u-strasbg.fr/cgi-bin/qcat?J/A+A/375/539

determination of some bulk properties of their embedded populations. Unfortunately, detailed studies of their stellar components have been hampered so far by the heavy obscuration towards most of these regions, rendering both the ionized gas and the stars ionizing it unobservable at visible wavelengths. Observations in the near infrared, being much less affected by intervening extinction, can however overcome this limitation, providing detailed information on the properties of the stellar population and the distribution and dynamics of the interstellar medium.

As a first step in the study of their stellar components and the detailed morphology of their associated gas, we present in this paper a broad-band JHK imaging survey of compact HII regions in Cygnus X. The power of near-infrared imaging in a particular example, also located in Cygnus X, is demonstrated by the study of Comerón & Torra (1999) of the DR 18 HII region. The more limited observational material available in the present case, in particular the unavailability of narrow-band imaging centered on selected lines in the K band, does not allow us to go to the level of detail reached in our previous study of DR 18. However, it is still useful in revealing the morphology of the different HII regions and the diverse degrees of richness, concentration, and obscuration of the stellar aggregates that power them.

Our sample selection criteria, observations, and data reduction are described in Sect. 2. Section 3 presents the results and introduces our method for distance estimates. We also supply a detailed object-by-object discussion, placing each one in the context defined by previous observational work. Our conclusions are summarized in Sect. 4.

2. Observations

2.1. Target selection

Our target list was built using the catalog of compact radio sources in Cygnus X of Wendker et al. (1991). Based on the spectral index measured between 408 and 4800 MHz, that paper classifies the sources as thermal (HII regions) and non-thermal (supernova remnants). Only the first class was considered for the present study. Furthermore, we retained only those sources whose listed size was compact enough to be completely covered in the field of view of the detector used (see Sect. 2.1), thus rejecting HII regions whose listed size exceeded $5'$. Some of the sources meeting our two selection criteria have been intensively studied by other authors, also in the near-infrared, and therefore we excluded them from our target list as well. These sources are S106, DR21, and DR18. The targets in our final sample are individually discussed in Sect. 3.3, and their coordinates and main features are given in Table 1 at the end of this paper. For the sake of homogeneity we use the object denominations of Wendker et al. (1991), although some sources, noted in Table 1, also have more commonly used DR (Downes & Rinehart 1968) denominations.

2.2. Observations and data reduction

The observations presented in this paper were carried out on the nights of 6 and 7 August 1998 using CAIN, the near-infrared array camera at the 1.5 m Carlos Sánchez Telescope in the Observatorio del Teide (Canary Islands, Spain). This camera has a Rockwell 256×256 array with a pixel scale of $1''00$ per pixel at the K band (the scale depends slightly on the filter used), yielding a field of view of $4'2 \times 4'2$ per frame. Each observation of a region in a given filter consisted of 9 sequences of 5 individual frames each, obtained on a dither grid of 3×3 points in a square pattern of $20'' \times 20''$. The 5 individual frames at each position, each of 6 s of exposure time, were saved individually. This was preferred to stacking of the 5 exposures in a single frame, due to the appreciable drift in the positioning of the telescope during the 30 s spent at each position: blind tracking was used, as the frequency of offsets to complete the drift pattern would otherwise have imposed a large overhead in the execution time if using the autoguider. Shift-and-add at the reduction stage allowed us to compensate for the drift, as well as to remove cosmic rays and detector bad pixels in the stacked images. Sky images were obtained separately, as the crowdedness of our target fields and the abundance of extended nebulosity did not allow us to construct acceptable sky background images by median-filtering of the jittered exposures on the target fields. The observing strategy employed was as follows: first, all the HII regions were imaged in the K filter, in a sequence consisting of one observation of one field, a nearby sky region, another field, the sky region again, and so on until observing all the fields in our list. Then, the sequence was repeated in the H filter, and finally in the J filter. Photometric calibration was obtained from short exposures of each field in each filter on both nights when the Cygnus X region was near the meridian, alternating the exposures of the fields with observations of the infrared standard star FS 29 (Casali & Hawarden 1998).

The observations were reduced using standard infrared imaging data reduction procedures, implemented by means of dedicated IRAF scripts. The small variations in the scale of the images obtained through the different filters were corrected for by enlarging the images in the J and H filter so as to match the scale of the K image, using a flux-conserving pixel interpolation schema. Point sources were detected by adding the frames in J, H, and K, and running DAOPHOT (Stetson 1987) on the resulting image. The photometry was obtained as follows: in a first step, aperture photometry with a large aperture was performed on the images of the standard star and of suitable bright and isolated stars in the short exposures of the fields imaged at the same time as the standard. This allowed us to set up a network of bright secondary standards in each field and filter. Then, aperture photometry with a small aperture (3 pixels in radius), adequate for our rather crowded fields, was performed on the deeper images. Finally, magnitudes for all the stars detected in each field were determined taking those of the secondary

standards as a reference. We also experimented with results obtained by performing point-spread function (PSF) photometry on the deeper images. However, we found that individual zeropoints obtained from the comparison between PSF photometry of each secondary standard in the deep exposures and aperture photometry in the calibration exposures yielded a considerably larger scatter than when comparing the latter with small-aperture photometry in the deep exposures. The complete list of positions and magnitudes of stars in each region is available electronically only as Table 2 through the Centre de Données Stellaires (Strasbourg, France).

3. Results

3.1. Images, color-color, and color-magnitude diagrams

A representative sample of our main results can be seen at a glance in Fig. 1, showing images of two selected regions in the J, H, and K filters. The full Fig. 1 (available only in the electronic version of this paper) presents a JHK color composite of each region imaged. Most of the regions show some degree of stellar clustering and a definite extent of the nebula, and only two of them (ECX6-4 and ECX6-26) do not show any signs of either a stellar density enhancement or of nebulosity. Individual images of some regions showing structures in greater detail are presented in Sect. 3.3 when adequate.

It is possible in most cases to roughly delimit the extent of the stellar aggregate near the center of each HII region, allowing us to concentrate in a small area dominated by the population ionizing it. Our choice of the boundaries of the ionizing aggregate in each case where it is easily identified is presented on the K-band image in Fig. 1. Color-magnitude and color-color diagrams are also presented for each region, with the exception of ECX6-7a due to a heavily saturating star that does not allow us to obtain useful photometry. Marked with larger symbols in the diagrams are the stars within the boundaries assigned to the ionizing aggregates. Needless to say, such a definition of the boundaries is highly arbitrary and surely includes within them many stars unrelated to the aggregate. Nevertheless, we have tried to be deliberately conservative when deciding on the boundaries to avoid the opposite, namely that stars that may substantially contribute to the ionization of the HII region may be left outside them. This is of some importance in the ensuing discussion on distance estimates.

3.2. Distance estimates

A well known drawback with the use of kinematical distances in the direction of Cygnus is the near-zero radial velocity gradient up to ∼2 kpc from the Sun. On the other hand, spectroscopic distances for the heavily obscured member stars are very difficult to obtain. Here we propose to combine published radio continuum fluxes together with a few assumptions on both the ionized gas and the stellar component to obtain rough estimates of the distance to each region.

Let us assume that most of the stars within the areas outlined in Fig. 1 belong to the HII regions. We assume moreover that foreground and background stars have dereddened apparent magnitudes fainter than those of the brightest members of the HII region. In other words, we assume that, in an unobscured view of the HII region, the brightest stars would be physical members of it. Finally, we assume that all the stars contributing to the ionization appear in our images and that there are no undetected massive stars. To correct approximately for reddening, we assume that all the stars in the area have early spectral types and thus their intrinsic color are confined to a narrow range. We determine the reddening using $(H-K)$ that, although more likely to be affected by circumstellar emission, is available also for the most reddened stars that are undetected at J. The bias introduced by K-band excess is discussed at the end of this section. Assuming an average intrinsic color $(H-K)_0 = -0.04$ for OB stars (Tokunaga 2000), the extinction at H, A_H, is

$$A_H = 0.11 + 2.78(H-K) \quad (1)$$

where we use the extinction law of Rieke & Lebofsky (1985). The dereddened H magnitude, $H_0 = H - A_H$, is related to the monochromatic flux F_H emitted by the star by

$$F_H = (4\pi D^2)\ 1.14 \times 10^{(-6-0.4H_0)}\ \mathrm{erg\ cm^{-2}\ s^{-1}\ \mu m^{-1}} \quad (2)$$

where D is the distance to the star and use is made of the absolute flux vs. H magnitude calibration (Bessell et al. 1998). Following evolutionary models of massive stars by Schaerer & de Koter (1997) relating effective temperature T, stellar radius R, and photoionizing flux Q_0 below the Lyman limit as a function of main-sequence spectral type, and assuming that the star radiates like a black body at H, the relationship between Q_0 and F_H for individual stars is approximately

$$\log Q_0(\mathrm{s^{-1}}) = -64.1 + 3.15 \log F_H(\mathrm{erg\ s^{-1}\ \mu m^{-1}}). \quad (3)$$

The numerical coefficients are set so as to match the models at spectral types B0.5 and O3, with a maximum offset around O8 where Eq. (3) yields a Q_0 that is only 0.70 times the model prediction. This offset has a small influence on the distance determination, leading to an underestimate that never exceeds 10% and can be neglected relative to other sources of uncertainty. Replacing Eq. (2) in Eq. (3), the ionizing flux supplied by an aggregate of N stars is:

$$Q_0(\mathrm{s^{-1}}) = 1.06 \times 10^{56} D^{6.30}(\mathrm{kpc}) \sum_{i=1}^{N} 10^{-1.26 H_{0_i}}. \quad (4)$$

For an ionization-bounded HII region with an electron temperature of 10^4 K and being optically thin at frequency ν, the continuum flux is (Altenhoff 1960):

$$Q_0(\mathrm{s^{-1}}) = 1.8 \times 10^{46} \nu^{0.1}(\mathrm{GHz}) D^2(\mathrm{kpc}) S_\nu(\mathrm{Jy}). \quad (5)$$

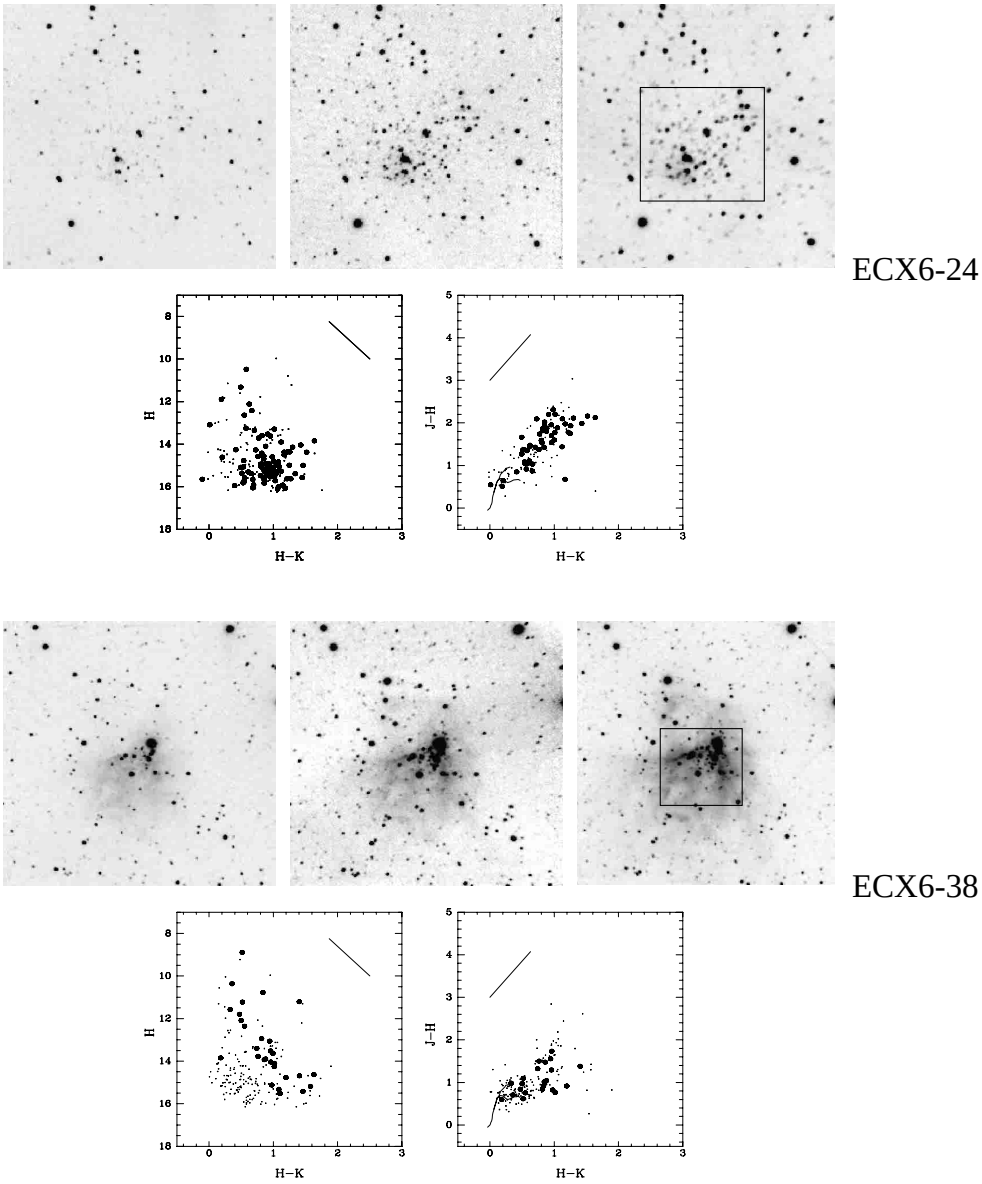

Fig. 1. Images, color-magnitude, and color-color diagrams of each region (the full sample can be found in the electronic version of this paper only). Selected samples are shown in the printed copy, where J (left), H (center) and K (right) images are presented for ECX6-24 and ECX6-38. The images display an area of $4'2 \times 4'2$ around the position of the emission peak at 4.8 GHz, as listed in Table 1. North is up, East to the left. The boundaries that we propose for the ionizing stellar aggregate are outlined in the K-band image when such an aggregate can be discerned. No color-color and color-magnitude diagrams are presented for ECX6-7a, due to the presence of the heavily saturating star BC Cyg. In the color-magnitude and color-color diagrams each dot represents a star in the field, and filled circles are stars within the adopted boundaries of the aggregate. The straight lines in the diagrams represent the direction and amount of the shift in the position of a star caused by a visual extinction of $A_V = 10$ mag, according to Rieke & Lebofsky (1985). The curves in the color-color diagrams mark the *locus* of unreddened main sequence stars (bottom branch) and giants (upper branch) using intrinsic colors from Bessell & Brett (1988). This *locus* is not marked in the color-magnitude diagrams, as the distances are unknown, but the early-type type stars of interest in the present work would lie if unreddened along a nearly vertical line at $H - K \simeq -0.04$. To minimize the scatter due to faint stars near the detection limits and to spurious detections, only stars with errors $(\Delta H, \Delta K) < 0.2$ mag are represented in the color-magnitude diagrams, and with $(\Delta J, \Delta H, \Delta K) < 0.2$ mag in the color-color diagrams.

The fluxes S_ν at different frequencies for all our HII regions can be found in Wendker et al. (1991). The distance is thus:

$$D(\mathrm{kpc}) = 5.346 \times 10^{-3} \left[\frac{\nu^{0.1}(\mathrm{GHz}) S_\nu(\mathrm{Jy})}{\sum_{i=1}^{N} 10^{-1.26 H_{0_i}}} \right]^{0.233}. \quad (6)$$

The three main possible departures from the assumptions described earlier make the distance calculated in this way a lower limit to the actual one. Indeed, contamination by non-members in the direction of the HII regions adds undue terms to the summation in Eq. (6), with N exceeds the actual number of members of the ionizing aggregate.

In some instances we can reduce this contamination by excluding likely foreground stars due to their much bluer colors. However, the assumption that the brightest stars in the field after dereddening belong to the HII region becomes less likely as distance increases, and prevents distance estimates beyond the local arm (where kinematic distances do become reliable instead). On the other hand, if a HII region is density- rather than ionization-bounded, the ionizing photons leaking out of it turn Eq. (6) into an inequality where the left-hand term exceeds the right-hand one. Similar arguments apply if dust in the HII region absorbs a fraction of the ionizing photons. The third assumption concerns the possibility of K-band excesses. If this excess exists, Eq. (1) overestimates the extinction and thus also the flux contributed by the star, again overestimating the value of the summation in Eq. (6) and leading to an underestimate of the distance. All these cases go in the same direction, underestimating D by factors difficult to evaluate. However, as will be discussed below, the distances obtained in this way are often found to be comparable to those given in the literature and derived by independent methods. This suggests that the assumptions of ionization-bounded HII regions, of domination of physical members of the aggregate in the selected areas, and of negligible K band excess are essentially valid in many cases. On the other hand, an effect that can seriously produce an *overestimate* of D is the non-fulfillment of our third assumption above, namely that no stars significantly contributing to the ionization are too obscured to escape detection in our observations. This is a more serious concern in the case of the youngest, unevolved regions which may contain some of its most massive stars still embedded in their parental clouds. Some actual examples from our sample in which this is likely to happen are noted in Sect. 3.3.

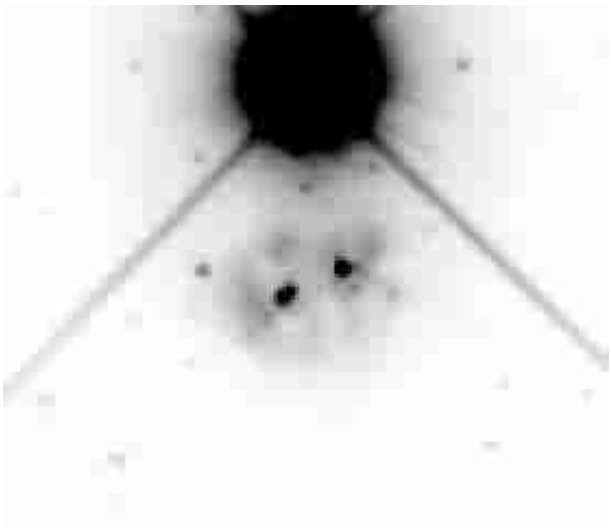

Fig. 2. A close-up view of the nebula near ECX6-7a in the K band. The dynamic range has been increased over that of Fig. 1 to clearly show the two bright red stars contained in the nebula.

3.3. Discussion on individual regions

3.3.1. ECX6-4

Wendker et al. (1991) list this source as unresolved at 408 and 4800 MHz, and suggest a possible association with DM+38 4000, a O6.5V((f)) star in the Cygnus OB1 association (Mathys 1989). This is the brightest star of our field in K, appearing slightly below and to the right of the image in Fig. 1. We do not detect any signs of clustering or nebulosity in our images, while the color-color and color-magnitude diagrams look markedly different from those that we derive for all the other regions included in the present study. The absence of strongly reddened sources in this field suggests that the line of sight is relatively extinction-free up to large distances, so that any significantly reddened sources in that direction are too distant to have been recorded in our images. This would also apply to the HII region if it is not associated with DM+38 4000. The long distance would most probably place it in the Perseus arm, implying a large negative radial velocity. Unfortunately, ECX6-4 does not appear in any of the existing emission-line surveys of the region, thus preventing us from verifying its membership in either the Perseus or the local arm. It should be noted however that its relatively high galactic latitude, $+1°66$, would imply a distance greater than 200 pc to the galactic plane at the distance of the Perseus arm. Given the positional coincidence and the lack of any other indications of clustering or nebulosity in the area, we favour the proposed association between ECX6-4 and DM+38 4000.

3.3.2. ECX6-7a and 7b

ECX6-7a and ECX6-7b are two HII regions probably related to the cluster Berkeley 87 (Turner & Forbes 1982). Berkeley 87 stands out as one of the most interesting and nearby regions of very massive star formation, with coexisting members that illustrate some of the main stages of stellar evolution in that regime. Among them are the WO star ST3 (Pitault 1981; Polcaro et al. 1997); the bright M3.5Ia supergiant BC Cyg (Jura & Kleinmann 1990); the B supergiant HDE 229059, possibly a close binary blue straggler of Cygnus OB1 (Mathys 1987) and the very peculiar variable V 439 Cyg (Polcaro & Norci 1998). A prominent structure likely to belong to Berkeley 87 is ON2, a massive star forming region containing compact HII regions and high density molecular clouds (Elldér et al. 1969; Matthews et al. 1973; Matthews et al. 1986; Dent et al. 1988; Polcaro et al. 1997; Shepherd et al. 1997, and references therein). Interactions between the stellar wind of ST3 and the interstellar medium associated to ON2 or Berkeley 87 has been proposed to be at the origin of the high energy emission observed in that direction of the sky (Polcaro et al. 1991; Manchanda et al. 1996). ECX6-7a and 7b are only two of the compact HII regions observed in this complex (Dent et al. 1988).

ECX6-7a is detected in our images as a bright, compact infrared nebula only 45″ South of BC Cyg, in the outskirts of the Berkeley 87 cluster according to the boundaries proposed by Turner & Forbes. The compact radio source at the position of ECX6-7a has been identified in many previous studies (e.g. Wink et al. 1982; Lockman 1989), and is also a strong IRAS source that has eventually been classified as an ultracompact HII region (Churchwell et al. 1990). OH emission at its position has been detected by Cohen et al. 1995. High-resolution radio continuum observations by Garay et al. (1993) reveal a morphology similar to that seen in our infrared images, that Garay et al. tentatively classify as shell-like. The radio continuum flux has been attributed to an embedded O6 star. We note however that this stems from the adoption of a distance of 4.1 kpc to this region, close to the "far" value allowed by the distance ambiguity. Its likely association to Berkeley 87 and related objects suggest instead a much closer distance, of order 900 pc (Turner & Forbes 1982), and the corresponding ionizing flux would therefore be closer to that of a B0 star. Our H and K band images reveal two very red point sources with $K \sim 9$ (the precise value cannot be determined due to the proximity to BC Cyg, which is heavily saturated in our images) near the center of the nebula, which could correspond to the ionizing sources; see Fig. 2 for more details. Assuming that the depth of Berkeley 87 is of the order of its radius, the physical separation between BC Cyg and ECX6-7a should be ∼2 pc at most if both objects indeed belong to the cluster. The coincidence in the projected positions of an evolved star like BC Cyg, aged 6–7 Myr (Turner & Forbes 1982) and a compact HII region like ECX6-7a where star formation is much more recent or even still going on argues for a complex evolutionary story of Berkeley 87, with nearly contiguous star forming sites evolving at markedly different speeds, as opposed to a more or less ordered wave of star formation moving as a definite pattern across the cloud.

ECX6-7b is more centrally located with respect to the main body of ON2. JHK imaging shows ECX6-7b as a moderately reddened, compact nebula approximately 1′3 across containing an embedded cluster that is apparent only in H in K. The three bright, lightly obscured stars of $J \sim 8.5$ that appear less than 1′ Southwest of the core of the nebula are probably unrelated foreground stars, as their colors are bluer than those of most stars in the central cluster. We have nevertheless included them within the area of the cluster in Fig. 1, and they appear as the three dots at the top left of the color-magnitude diagram. We find stars with largely varying degrees of reddening both in this area and outside it, reaching extinctions of up to $A_V = 30$ mag as derived from the color-color diagram. On the other hand, the brightest stars in the cluster tend to appear to the right of the reddening sequence in Fig. 1, indicating substantial amounts of circumstellar emission in the K band.

A comparison with the high resolution maps in ^{12}CO, SiO, H^{13}CO and SO_2 of Shepherd et al. (1997) shows that the reddened cluster of stars and nebulosity that appears in our JHK images is actually immediately Southwest of the main concentration of high density tracers, which is otherwise invisible in the near-infrared images. ECX6-7b may thus be a blister HII region where newly formed stars are disrupting the dense molecular cloud that still composes the core of ON2. Very high resolution observations by Hofner & Churchwell (1996) reveal a complex of three water masers associated with a subarcsecond-sized cometary ultracompact HII region near the interface between the core of ON2 and the near-infrared cluster. Possibly variable methanol emission is also detected in the region (Menten 1991; Szymczak et al. 2000), although the lower resolution of those observations prevents an accurate identification. It is interesting to note that exactly at the position of water masers numbers 1, 2, and 4 studied by Hofner & Churchwell, we detect an extremely red point source with $K = 13.3$, $H - K \simeq 4.2$[1] which may be its near-infrared counterpart (Fig. 3). This offers the potential of spectroscopically studying the deeply embedded star, a possibility rarely found (Watson & Hanson 1997). Another very red source ($K = 12.9$, $H - K = 2.9$) appears 15″ to the West-Southwest of it. Two other water masers

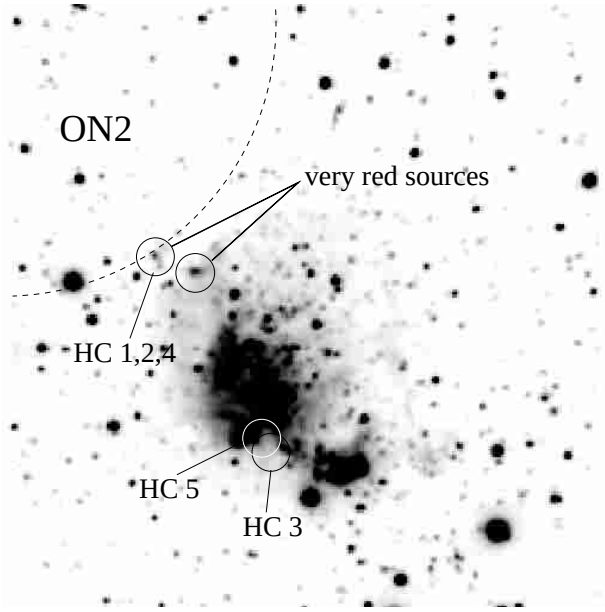

Fig. 3. A detailed view of ECX6-7b and the field around it in K. The dashed line roughly shows the boundary of ON2 as traced by ^{12}CO($J = 1 \rightarrow 0$) emission (Shepherd et al. 1997). The very red sources mentioned in the text are marked. The leftmost one is coincident with three water masers reported by Hofner & Churchwell (1996); the "HC" initials in the picture refer to the masers listed in that paper. The positions of two other water masers without obvious near-infrared counterparts are also noted.

[1] We prefer to give in our descriptions of individual objects the K magnitude, which is generally determined with better precision than H, especially in the case of very red sources. However, since the latter is expected to be less affected by circumstellar emission, we have preferred to use it in the vertical axis of the color-magnitude diagrams.

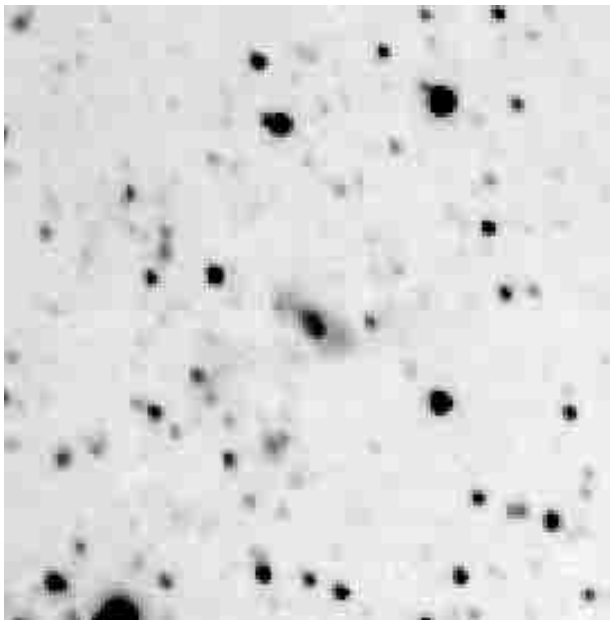

Fig. 4. A detailed view of the red, compact object at the position of ECX6-11 (K-band image), showing an extended, bilobular structure around the central source which is barely resolved.

mapped by Hofner & Churchwell (1996) appear closer to the core of the infrared nebulosity, but without an obvious near-infrared counterpart.

In view of the evidence on the complexity of this region and the existence of essential components undetected in our images, our distance estimate of 0.7 kpc is probably not very meaningful. Due to the marginal detection at H and the impossibility of obtaining a reliable estimate of the reddening, the near-infrared counterpart of the ultracompact component is not included in our census of ionizing stars, although it may be the dominant contributor to the radio continuum flux measured by Wendker et al. (1991). On the other hand, some of the sources for which we find the brightest dereddened magnitudes fall below the reddening sequence in Fig. 1, probably indicating that the K-band flux is dominated by circumstellar emission. Since these effects move our distance estimate in opposite directions, we regard our value of 0.7 kpc as very uncertain. The reasonable proximity to the value of 0.9 kpc proposed by Turner & Forbes (1982) for Berkeley 87 is thus probably fortuitous.

3.3.3. ECX6-11

No obvious cluster is seen at the position of this source, but right at the center we find a very red extended source, seen in detail in Fig. 4, whose position is coincident with that of the ultracompact HII region IRAS 20220+3728. This object appears in numerous studies of molecular line and radio continuum emission, having been detected in NH_3 (Molinari et al. 1996) and HCO^+ (Richards et al. 1987); see Chan et al. (1996) for a compilation of data. Moderate-velocity ^{12}CO emission is detected by Shepherd & Churchwell (1996). No water maser emission is detected at its position (Palla et al. 1991), but weak emission is detected approximately $1'$ North of it at a location where no obvious counterpart is visible in our images (Scalise et al. 1989). The LSR velocity of this component, -35.4 km s^{-1}, is very different from that measured at the position of IRAS 20220+3728 (-2.7 km s^{-1} from NH_3 lines, and similar values from other observations), indicating that both sources are probably unrelated.

VLA observations by Kurtz et al. (1994) at 3.6 and 2 cm reveal a complex, multiple-peaked morphology with an overall shell-like arrangement. The peaks are also identified in VLA observations at 6 cm by Molinari et al. (1998). The shell has two bright caps readily visible in the 3.6 cm map of Kurtz et al. which approximately coincide with the elongation in the NE-SW direction that the source has in our K band image. Interestingly, the minimum of emission at centimeter wavelengths coincides with the almost point-like bright nucleus seen in our H and K images ($K = 12.3$, $H - K = 2.4$). The comparison between the near-infrared and centimeter observations suggests a shell morphology for this very compact HII region, producing a bright rim detected in the VLA images and a not very obscured center that dominates the near-infrared image. The marginally resolved appearance of the core suggests that the emission from the nucleus is not purely stellar.

Despite the compact aspect of ECX6-11 in our images, several very red objects are seen within a $1'$ radius of it, the two most extreme having $K = 13.6$, $H - K = 3.1$ and $K = 14.4$, $H - K \sim 3.3$. This may mean that ECX6-11 is a member of a highly obscured cluster whose other members do not possess the massive dust envelopes that cause the bright IRAS-detected emission of the former. The color-magnitude and color-color diagrams of the region also shows a large scatter in reddenings and a few objects occupying the region of circumstellar excess.

A kinematical "far" distance of 4.0-4.5 kpc to ECX6-11 has been adopted in most works. Using the photometry of the central, marginally resolved source given above in combination with the 4.8 GHz flux of Wendker et al. (1991) and applying Eq. (6), we obtain a distance $D \simeq 1.2$ kpc, thus suggesting that the "short" solution to the distance ambiguity should be used instead. Nevertheless, the ionizing flux estimated by Molinari et al. (1998) using the "far" distance is only $Q_0 \simeq 8 \times 10^{47}$ s^{-1}, corresponding to a B0 ionizing star (Schaerer & de Koter 1997). Reducing the distance to 1 kpc would imply a decrease in Q_0 by a factor of 20 and an even later spectral type, ∼B2. We thus believe that the lower limit obtained from the application of Eq. (6) may be a large underestimate of the distance in the present case, perhaps due mostly to a substantial contribution of circumstellar emission to the near-infrared photometry or to substantial absorption of ionizing photons by dust.

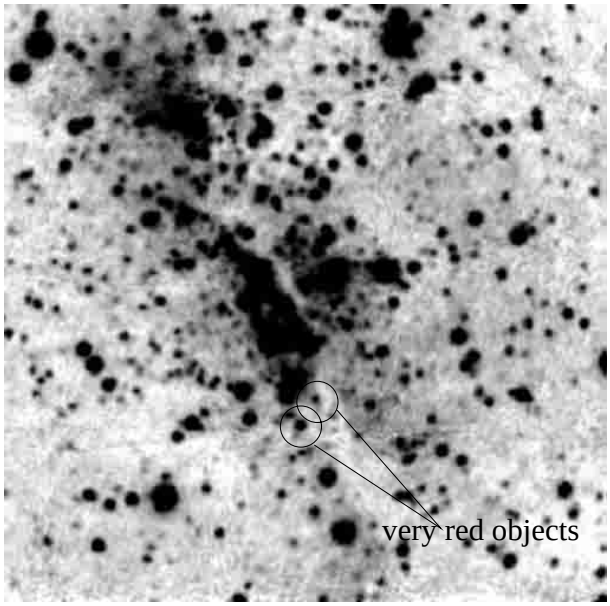

Fig. 5. An enlarged view of the K-band image of ECX6-15 (=DR6) with a reduced dynamic range to emphasize the nebulosity and the distribution of obscuring material. The position of the two faint, very red sources mentioned in the text is marked.

3.3.4. ECX6-12

ECX6-12 appears in our images, shown in Fig. 1, as a small ring-shaped nebula with a diameter of $\sim 50''$. The color-magnitude diagram shows that most of the objects in the area of the nebula are moderately reddened, with $E[H-K] \sim 1-2$ mag. Curiously, most of the objects in the area of the nebula seem to have circumstellar excess. This suggests a substantial underestimate of the distance as derived from Eq. (6), which at 1.7 kpc is already relatively large. This is confirmed by the kinematics of its radio recombination lines, whose LSR velocity is -28.2 km s^{-1} (Lockman 1989) clearly indicating membership in the Perseus arm. ECX6-12 appears in different radio continuum galactic plane surveys, but no detailed studies on it or its immediate surroundings appear to have been published to date.

3.3.5. ECX6-15

This source is best known as DR 6, one of the compact components of the IC 1318 complex. DR 6 is located between IC 1318b and c (Campbell et al. 1981). The region appears extended in the IRAS bands (Odenwald & Schwartz 1993), but its far-infrared emission (Odenwald et al. 1986) roughly coincides with the radio continuum size, $3'7 \times 2'9$ (Wendker et al. 1991). The latter matches well the size of the nebulosity seen in our images. A close correlation between the shape of the nebula in the infrared images and that mapped at 6 cm with the VLA by Odenwald et al. (1986) is seen. The most remarkable difference between both is the dark ridge crossing our images from SW to NE, roughly at the position where the centimeter emission peaks, showing that most of the radio continuum flux comes from a region obscured by a thick dust lane (see Fig. 5). On the other hand, concentrations "C" and "E" in the 6 cm map of Odenwald et al. are not easily identified in our images, although two very red sources ($K = 13.5$, $H-K = 2.7$ and $K = 15.3$, $H-K \sim 2.8$) are seen in the direction of concentration "C". This suggests the existence of large column densities of dust in those directions as well.

Due to the large extent of the nebula and the richness of the field, our "member selection" criterion may be including many foreground stars in the census of possible ionizing stars when trying to compute the distance. Despite this, our estimate of 1.0 kpc is consistent with its association to the IC 1318 complex (distance 1.5 kpc, consistent with the LSR velocity of -0.7 km s^{-1}; Odenwald & Schwartz 1993). The color-magnitude and color-color diagrams in Fig. 1 show a large scatter of extinctions, roughly between $A_V = 0$ and $A_V = 25$ mag. Most stars lie along the band defined by normal reddened main sequence stars, and a few moderately reddened objects in the region of circumstellar excesses. The overall picture of DR 6 as a cluster of HII regions powered by early B stars proposed by Odenwald et al. (1986) is consistent with our near-infrared observations.

3.3.6. ECX6-18

ECX6-18 is the DR 7 complex. At first sight, many characteristics of the radio continuum and far infrared emission are similar to those of DR 6 (Odenwald et al. 1986), but the distances to both complexes are very different as seen from highly negative radial velocity of DR 7 (-40 km s^{-1}; Piepenbrink & Wendker 1988; Lockman 1989). The kinematical distance, about 7.5 kpc, places it in the Perseus arm and about five times farther than DR 6. A distance significantly larger than that of DR 6 is also indicated by our non-kinematical estimate of $D > 3.6$ kpc. In our infrared images (Fig. 1) the nebulosity is evident in H and especially K, with all its area covered with faint red stars. Nothing is seen at visible wavelengths, where the field surrounding DR 7 is pervaded by tenuous nebulosity but not at the position of the region itself. The color-magnitude diagram shows the existence of many faint stars at the position of the nebula with varying amounts of reddening. No object is detected with large K-band excess. Like in the case of DR 6, the overall shape and extent of the near infrared emission is coincident with that of the radio continuum, except for the fact that the strongly peaked component "B" of the maps of Odenwald et al. (1986) is much less conspicuous in our images, where it appears near the Eastern edge. The much redder color that we appreciate in this component when comparing to the rest of the nebulosity probably indicates that it lies behind a screen of higher extinction.

Two ultracompact HII components have been detected in DR 7 (Kurtz et al. 1994). We detect a barely resolved

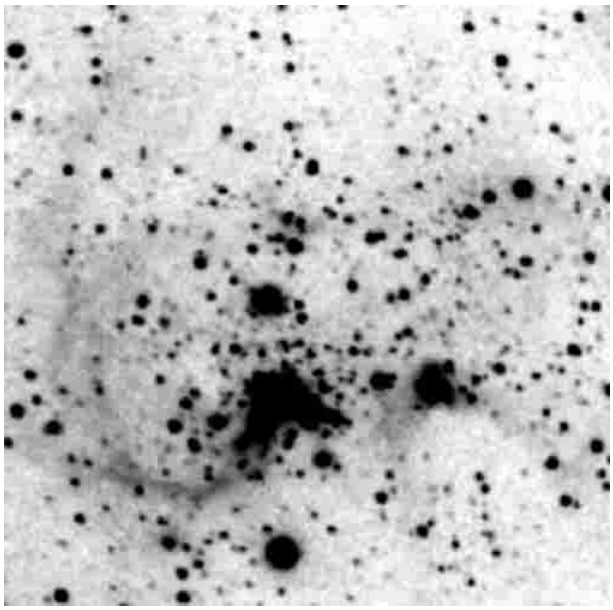

Fig. 6. An enlarged view of ECX6-20 in the K band, showing in more detail the arc-shaped extended emission described in the text.

red source at the position of one of them, G79.320+1.313, with $K = 12.6$, $H - K = 2.6$, $J - H = 2.1$. The other one is undetected in our images, and lies at the position of concentration "B" in the radio continuum map of Odenwald et al. (1986). The higher foreground extinction towards this concentration, as noted above, may be the reason for the non-detection of this second ultracompact component. None of these ultracompact sources has been detected to have associated water or methanol maser emission (Codella et al. 1996; Slysh et al. 1999).

The large size of DR 7 implied by its kinematical distance and the apparent extent of 2.5 arcmin that it has in our images qualifies it as a classical, Orion-like HII complex, rather than as a compact one as may be expected from the size-based selection criterion of our sample if belonging to the local arm.

3.3.7. ECX6-20

The region ECX6-20 is dominated by a very compact, moderately reddened cluster whose three brightest stars have $K = 10.1$, $H-K = 0.8$; $K = 10.2$, $H-K = 0.7$; and $K = 9.2$, $H-K = 0.30$. These are components of the multiple system CCDM J20296+3901C (Dommanget 1983). Two other, less conspicuous clusters are visible in the infrared frames as well, one to the West dominated by a star of $K = 11.6$, $H - K = 1.1$, and another one to the North with two stars of $K = 9.8$, $H - K = 0.7$ and $K = 9.3$, $H - K = 1.2$ respectively. Its velocity (-5.5 km s^{-1} from radio recombination lines, Lockman 1989; -2.9 km s^{-1} from associated CS emission, Bronfman et al. 1996) places it in the local arm, in consistency with our distance estimate (1.5 kpc) and with the low extinction in its direction.

An ultracompact component is detected in radio continuum observations in the direction of the main cluster (Kurtz et al. 1994), but the high stellar density with overlapping PSFs of bright stars in this region does not allow us to identify it in our infrared images. The ultracompact component is associated with extended emission mapped by Kurtz et al. (1999) that we also see easily in our K-band images (Fig. 6). The extended emission starts at the central cluster in the East-West direction and then bends Northwards, especially in the Eastern arm which is the most conspicuous one. Peaks in the centimeter emission are also seen in Kurtz et al.'s maps at the position of the two secondary clusters. An intriguing difference between the near-infrared and the radio continuum emission is that the former is much more narrowly confined to a ridge that outlines the Southern edge of the latter, giving it a clear arc-like appearance that is much less obvious in the radio continuum maps. The arc can be traced for almost 180° starting from the cluster and has a radius of $\sim 40''$ or >0.29 pc at a distance >1.5 kpc. The Western arm is much less visible both in the infrared and in the radio, and it contains the Western subcluster. The position of dense clusters at the edge of such an arc suggests that their formation might have been externally triggered by an energetic event that produced an expanding bubble around it (e.g. Elmegreen 1998).

3.3.8. ECX6-21

The most detailed study existing to date on ECX6-21 is that of Odenwald & Schwartz (1989), who were the first to note the association of IRAS 20286+4105, an IRAS point source with a steeply rising spectrum in the 12-100 μm range, with a nicely delineated elliptical ring in visible images. They obtained ^{12}CO($J = 2 \rightarrow 1$) observations able to resolve the object and provide kinematical information giving hints of radial motion or rotation of the ring, but without conclusive results on this point. The colors of the IRAS source are those of an ultracompact HII region, and its low resolution IRAS spectrum is typical of a HII region as well (Kwok et al. 1997). The IRAS source is likely to lie at the geometrical center of the ring, where emission from high density tracers such as NH_3 (Molinari et al. 1996) and CS (Bronfman et al. 1996) is detected. Water maser emission is also found at that position (Palla et al. 1991).

In our infrared images (Fig. 7) the ring is not seen so clearly as such, and it is interesting to note that its outline is somewhat less regular than in the visible. Its area is filled with very faint emission and a decrease in stellar density can be noted within its contour, indicating that the ring is filled with obscuring material. A very red source with $K = 15.5$ and undetected in H appears near the center, consistent with the position of the ultracompact component. Unfortunately, no published high resolution observations exist allowing a sub-arcsecond positioning of the ultracompact source, so the identification is tentative only. Other red sources appear just North of the moderate

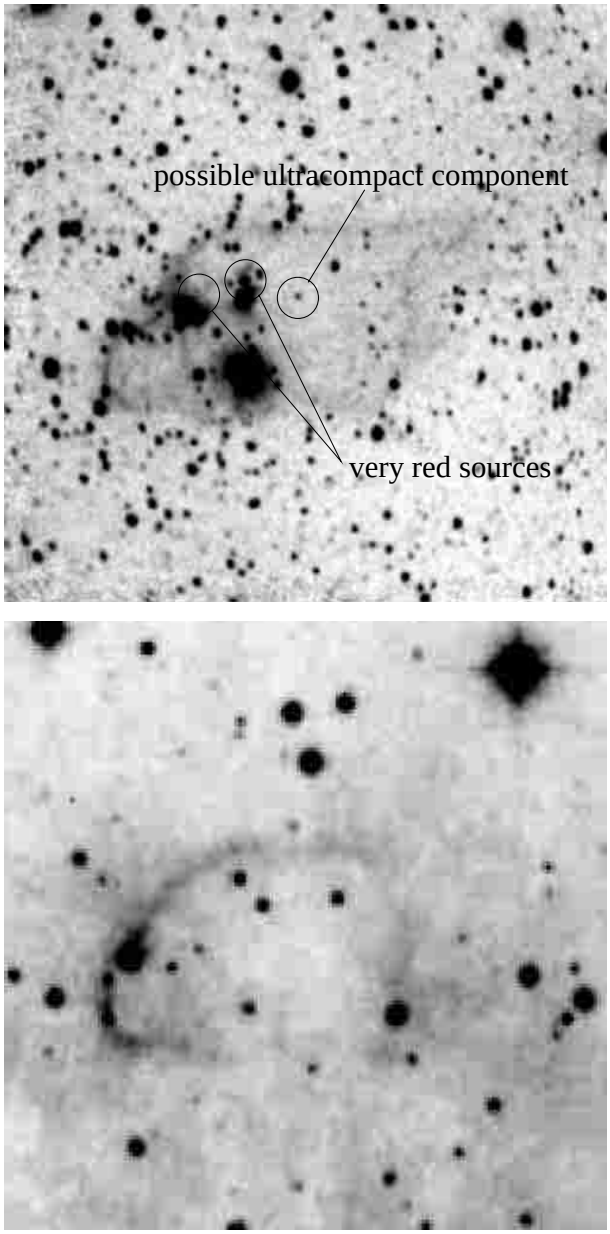

Fig. 7. An enlarged view of ECX6-21 in K, enhancing the nebulosity. The position of the very red source at the center of the ring that may be the counterpart of the ultracompact component is marked. Also noted are two very red sources referred to in the text. For comparison, an image of the same field at visible wavelengths from the Digitized Sky Survey is shown in the bottom panel.

concentration of stars near the Eastern edge of the ring. The Southernmost star of this group is a double with components having $K = 9.7$, $H - K = 0.6$, $J - H = 0.6$ and $K = 10.3$, $H - K = 1.1$, $J - H = 2.1$, respectively; only the bluer component appears in visible images as a rather inconspicuous object within the ring.

The radial velocity of ECX6-21, -3.9 km s^{-1} (Bronfman et al. 1996), places it in the local arm and is consistent with the lower limit of 1.0 kpc that we estimate. Although this is identical to the value of 1.0 kpc adopted by Odenwald & Schwartz (1989), our determination must be taken with special caution in this case, however: as indicated in Fig. 1, our distance estimate considers the brightest stars to the East of the ring, coincident with the brightest part of the nebulosity, as the ones causing the ionization, and neglects the contribution of the ultracompact component. On the other hand, two of the stars in the area with the reddest $H - K$ color have blue $J - H$ that could indicate circumstellar excess, and we may thus be overestimating their contributions to the ionizing flux.

3.3.9. ECX6-24

While nothing particular is seen in visible-light images of the area where ECX6-24 is located, near-infrared images reveal a fairly rich cluster of faint, moderately reddened sources (Fig. 1) clearly standing out over the stellar background. No heavily reddened sources or traces of nebulosity are seen in that direction: the associated radio source is so far identified only in radio continuum (Wendker et al. 1991) and radio recombination lines (Lockman 1989), with no indications of dense gas or embedded sources detectable by IRAS. The size and orientation of the radio-detected HII region (Wendker et al. 1991) are in good agreement with those of the cluster as seen in our images.

The LSR velocity measured by Lockman (1989) is -5.1 km s^{-1}, indicating that the region belongs to the local arm. This can also be inferred from its relatively high galactic latitude, 2°3. We believe that our estimated distance to the region in this case is more reliable than in the ones discussed so far, given the absence of evidence for unseen members of the cluster contributing to the ionization, and the dominance of the cluster population within the selected boundaries of the cluster expected from the density contrast with the background. We also note that the vast majority of stars that we consider as contributors to the ionization are located in the no-excess area of the color-color diagram, thus suggesting that our dereddening procedure is essentially correct in this case and does not result in a substantial underestimate of the distance. In view of this, the distance that we derive, 2.7 kpc, is likely to be near the true one. We note that such a distance, while still being consistent with membership in the local arm, places ECX6-24 behind most of the major structures in Cygnus X (Odenwald & Schwartz 1993).

3.3.10. ECX6-25

The region ECX6-25 = DR 15 has been studied in detail at far infrared, molecular line, and radio continuum wavelengths by Odenwald et al. (1990). The overall appearance in the far infrared (40–250 μm) shows a main peak of emission, related to their source FIR 1 (=IRAS 20306+4005), and a secondary peak to the Southwest, perhaps associated to IRAS 20293+3953. The latter is well outside the boundaries of our near-infrared images and is not discussed here. The appearance at visible wavelengths in the Digitized Sky Survey images shows a two-component

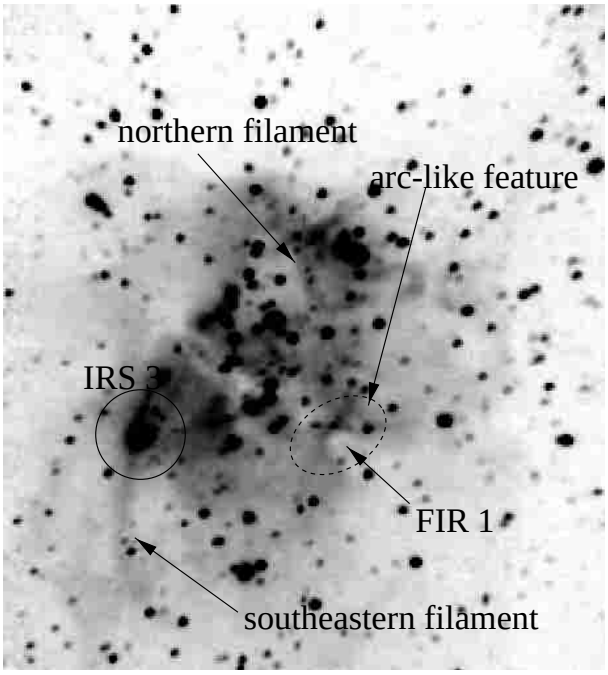

Fig. 8. A detailed view of ECX6-25 (K band) showing the position of the objects and features noted in the text.

structure in our field, a rather compact one to the Northwest and a diffuse one to the Southeast, with no visible nebulosity in between. The near-infrared images show that this is due to dust obscuration, revealing bright nebulosity joining both regions and a higher density of reddened stars in this region, probably a cluster physically related to DR 15. Only the densest parts of the dust lane are seen in the near-infrared image as a much thinner dark band that crosses the nebula from Northeast to Southwest. The VLA radio continuum maps of Odenwald et al. (1990) show a broad peak of the radio continuum emission roughly coincident with the center of the dark band.

A sharper peak of radio continuum emission coincides with the position of FIR 1, that lies at the Western edge of the dust lane and is not seen in our images. The K-band image shows however that the lane is disrupted near this position by a bright, arc-like feature with FIR 1 in its concavity, vaguely resembling a bow shock. This is shown in more detail in Fig. 8. At the position of FIR 1 Kurtz et al. (1994) have mapped an ultracompact component that appears elongated perpendicular to the direction of the dust lane at 3.6 cm, and is resolved into several aligned peaks at 2 cm, suggesting the presence of a collimated outflow. The high resolution maps of Kurtz et al. also suggest that collimation takes place at scales of $1''$ or less, while the dust lane can be traced in the infrared by at least $75''$. The existence of a large-scale disk-like feature, possibly associated with a hypothetical disk that may play an important role in collimating the outflow of the embedded object at the core of FIR 1, is reminiscent of the structure of another bipolar HII region studied in much more detail, S 106 (e.g. Roberts et al. 1995; but see also Barsony et al. 1989). Based mostly on morphological arguments, Odenwald et al. (1990) suggest that DR 15 may have formed as a result of the collision of two molecular clouds, giving rise in particular to FIR 1 at the collision interface. The sparse reddened cluster that we find in our near-infrared images may have formed as a consequence of this process as well. Kinematics does not provide much evidence for this scenario, although the discrepancies among observations of different components do suggest a rather complicated pattern of motions, at least in the vicinity of FIR 1: the LSR velocity measured by Lockman (1989) from recombination lines at low spatial resolution is +8.5 km s^{-1}, while ^{12}CO profiles in the direction near FIR 1 give components between −5 and 0 km s^{-1}. Also in that same direction, Bronfman et al. (1996) measure +3.7 km s^{-1} in the CS($J = 2 \rightarrow 1$) line. Other measurements in that range are quoted in Wendker et al. (1991).

Our infrared images also show hints of filamentary structure, the most conspicuous being a roughly semicircular arc that surrounds two bright stars in the Northern component and an extended wisp extending outwards at the Southeastern corner of the nebula. This wisp starts approximately at the position of IRS 1 (Kleinmann et al. 1979), a bright red source with $K = 8.9$, $H - K = 1.7$, $J - H = 2.7$. Interestingly, the radio continuum map does not show this filament, but a protuberance appears instead at the Southern edge, containing Kleinmann et al.'s source IRS 3. We hypothesize that this protuberance and the near-infrared filament may be a part of a single bubble-like structure, like the one that we described earlier in our discussion of ECX6-20, whose brighter part at radio wavelengths is too obscured for detection in our infrared images.

The color-color and color-magnitude diagrams show the existence of a mostly faint population of stars with extinctions ranging from 0 to ∼25 mag in the visible. Our distance estimate of 0.4 kpc in the present case is rather puzzling, as the region most surely lies considerable farther, probably at least in the far side of the Cygnus ridge as proposed by Wendker et al. (1991), at around ∼1 kpc. The star assumed to dominate the ionizing flux according to our prescription is IRS 3 (Fig. 8), that becomes the brightest star in the field after dereddening. Its colors show no indication of strong infrared excess, implying that our dereddening procedure should be approximately valid. On the other hand, the high resolution radio maps show that a large fraction of the centimeter flux is contributed by FIR 1, that is not detected by us and therefore is not taken into account in our census of candidate ionizing stars. For the reasons given at the end of Sect. 3.2, neglecting the contribution of FIR 1 should produce an overestimate of the distance, rather than an underestimate. The possibility that IRS 3 does not actually belong of DR 15, thus leading to a substantial underestimate of the distance, seems rather unlikely in view of its brightness, red colors, and location in the region. A possible explanation of the distance discrepancy might be that the

HII region is density bounded, with a large number of ionizing photons leaking out of it (Sect. 3.2). An alternative explanation based on absorption of a large fraction of ionizing photons by dust seems ruled out by the analysis of Odenwald et al. (1990), who concluded that the HII region inside FIR 1 is almost dust-free.

3.3.11. ECX6-26

Nothing obvious is seen at the position of ECX6-26 in our infrared images. This is a relatively faint, extended source in Wendker et al. (1991) also detected in other radio continuum surveys of the galactic plane. It may be associated to the infrared source IRAS 20316+4155, a possible young object near Cygnus OB2 (Parthasarathy et al. 1992). However, the lack of any additional information, in particular radial velocities or near-infrared detection, precludes any firm conclusion on its location and nature. The field where this source is located contains mostly faint stars with low-to-moderate reddening, the brightest star appearing in the Southeastern corner of our images having $K = 7.8$.

3.3.12. ECX6-27

The region ECX6-27 appears projected near the core of the Cygnus OB2 association, but the large negative radial velocity (-62.4 km s^{-1}, Lockman 1989; -66.4 km s^{-1}, Bronfman et al. 1996) exclude a possible physical link between both (see also Piepenbrink & Wendker 1988). The near-infrared images show two distinct concentrations separated by $\sim 75''$, corresponding to 3.5 pc at an assumed distance of 10 kpc for the outer arm where ECX6-27 probably lies. The main one (to the Northwest, just left and below the center of the image) coincides with the position of IRAS 20321+4112, an object with the mid-infrared colors of an ultracompact HII regions where CS emission is detected by Bronfman et al. (1996). However, most of the radio emission must be dominated by an optically thin component, as noted by Wendker et al. (1991) from the very shallow spectral index between 408 and 4800 MHz. The HII region is associated to an extended, cold HI cloud found at the same position and velocity (Wendker 1984). Our distance estimate of 3.3 kpc, while being the second highest in our sample, is most probably heavily contaminated by foreground stars.

3.3.13. ECX6-38

The HII region ECX6-38 is a bright compact nebula easily seen in wide-angle pictures of the North America-Pelican nebula complex, located $\sim 0^\circ 5$ West of the latter. Its location in the direction of that complex and in front of the Cygnus rift strongly suggest a distance of less than 1 kpc, consistent with the LSR velocity measured in radio recombination lines by Piepenbrink & Wendker (1988) and Lockman (1989) (-6.6 km s^{-1} and -8.5 km s^{-1}, respectively). The distance that we estimate, 0.8 kpc, is thus probably close to the actual value. The structure of this nebula is much more clear in our near-infrared images, where it displays a clear fan-shaped morphology opened towards the South-Southeast. Near the vertex of the fan a very compact cluster of moderately reddened stars is detected. Some of them can be seen at visible wavelengths, especially the brightest star in the cluster that has $V \simeq 10.5$. We measure $K = 8.4$, $H - K = 0.5$, $J - H = 0.6$ for this star and resolve a somewhat fainter companion about $1''5$ to the South.

The extent of the nebula, its surface brightness in the visible, and probably also its distance are similar to those of S 106, and in view of this it may seem somewhat surprising the large difference in attention that both have received so far. However, the structures of both nebulae are markedly different, as well as the characteristics of the stars responsible for the excitation. Despite of the existence of a compact cluster at the core of ECX6-38, most of the ionizing flux is most likely provided by the brightest star whose $VJHK$ magnitudes are given in the preceding paragraph. The dereddened H magnitude that we estimate, $\simeq$7.1, implies a spectral type around B2 at the distance of 700 pc, and thus an ionizing flux well below that supplied by the deeply embedded O9/B0 star that excites S 106 (Hodapp & Rayner 1991). The absence of any IRAS source associated to ECX6-38 indicates that it contains no bright embedded source and that our census of its brightest members is thus complete (Price et al. 1982 give fluxes at 11 and 20 μm for the associated source G84.0+0.8, but given the coarse resolution of their observations the association is doubtful; we thus give more weight to the IRAS non-detection).

Finally, it is interesting to note that the fan-shaped morphology with a compact cluster located at the vertex is very suggestive of a *champagne* blowout (Tenorio-Tagle 1979) produced when the initial HII region reached the boundary of the parental molecular cloud. On the other hand, the bright rimmed appearance of the opening of the fan suggests that it is filled with a rarified medium such as a stellar wind, rather than a denser stream of ionized gas initially in the cloud (Comerón 1997). The compactness of the cluster as compared to the overall extent of the nebula, as well as the apparently simple geometry, suggest ECX6-38 as an appropriate case study for the modeling of the dynamical interaction between moderately massive stars and the interstellar medium. Such a study would greatly benefit from high resolution radio continuum maps and kinematical information such as that currently available for many of the regions studied here.

4. Summary and conclusions

We have described the results of our JHK imaging survey of compact HII regions in the direction of the Cygnus X molecular complex. Observations at these wavelengths are largely unimpeded by dust extinction and are optimally suited for simultaneously studying both the nebulosity

Table 1. Summary of characteristics of the regions studied.

Name	α (2000)	δ (2000)	Distance (Eq. (6))	Description
ECX6-4	20:18:31.1	+38:51:22		No nebula or cluster. Probably associated to the O6.5V((f)) star DM+38 4000
ECX6-7a	20:21:39.1	+37:31:17		Compact, in Berkeley 87, near M supergiant BC Cyg
ECX6-7b	20:21:41.3	+37:26:10	0.7 kpc	Possible blister in ON2, ultracompact component detected in K
ECX6-11	20:23:55.7	+37:38:13		Isolated and elongated. Ultracompact component at the center marginally resolved
ECX6-12	20:25:23.2	+37:23:10	1.7 kpc	Ring-shaped, in Perseus arm. Distance underestimated from Eq. (6)
ECX6-15	20:27:13.0	+39:26:08	1.0 kpc	DR 6. Cluster with bright amorphous nebulosity
ECX6-18	20:28:10.1	+40:52:00	3.6 kpc	DR 7. Amorphous nebulosity, cluster of faint stars, in Perseus arm. Distance underestimated from Eq. (6)
ECX6-20	20:29:37.1	+39:01:59	1.5 kpc	Compact aggregate at the center, large arcs extending from it
ECX6-21	20:30:27.1	+41:15:40	1.0 kpc	Ring-shaped in visible, filled with emission in K. Possible central ultracompact source seen in K
ECX6-24	20:32:21.7	+43:41:12	2.7 kpc	Well-defined cluster, no apparent nebulosity
ECX6-25	20:32:31.2	+40:16:35	0.4 kpc	DR 15. Large-scale arcs, rich aggregate. Ultracompact component undetected
ECX6-26	20:33:23.0	+42:04:47		Nothing obvious detected
ECX6-27	20:33:55.3	+41:23:03	3.3 kpc	Double concentration with faint reddened stars. In outer arm behind Cygnus OB2, distance underestimated from Eq. (6)
ECX6-38	20:45:38.9	+44:15:09	0.8 kpc	Near Pelican nebula, compact cluster at center of fan-shaped bright nebulosity, probably blister-like

and the stars ionizing it. Our images illustrate indeed a large variety of morphologies among the former, and reveal aggregates of varying richness among the latter. A very brief summary of the main characteristics of each region is given in Table 1 to illustrate this diversity.

We have provided rough non-kinematical estimates of distances to our targets, based on a comparison of the stellar contents to the radio continuum flux, that are also listed in Table 1. In practice, the validity of the method is limited by a number of assumptions concerning membership, dereddening, and completeness of the stellar component. Actual cases in which these assumptions appear to be invalid or in which unrealistic distances are obtained have been discussed.

Our descriptions of individual regions in the light of previously published material in other domains stress the importance of multiwavelength observations in disclosing their structures and the relationship between their stellar and gaseous components. A variety of morphological features (bubble-like, ring-shaped, arc-shaped, fan-shaped) are revealed by our images that are not seen at other wavelengths and resolutions. Such features suggest these regions as test cases for models of the dynamical interaction between the energetic output of massive stars and their surrounding gas. On the other hand, the observations presented here provide likely near-infrared counterparts of a number of known ultracompact HII regions, which appear unresolved or only barely resolved at an arcsecond scale, implying linear sizes of order $\sim$0.01 pc or smaller. The new detection at K of these objects, so far observed only in the radio domain, suggests that spectroscopic studies of the embedded star or its immediate surroundings should be possible, thus providing a valuable complement to the existing radio observations.

We conclude by pointing out that the broad band, survey nature of our near-infrared observations leaves much room for follow-up detailed studies in the same spectral region. Narrow-band imaging through selected filters would be very helpful in exploring the nature of the extended emission, and particularly in separating the respective contributions of recombination emission, H_2 deexcitation, and continuum emission of small heated grains, leading to a much better characterization of the physical and dynamical conditions in the nebulae. On the stellar side, higher resolution imaging is needed for improved photometry, given the crowdedness of the fields. At the same time, deeper observations would be helpful to sample not only the lower-mass component of the associated aggregates, but also more deeply embedded massive objects that may not have been detected in our observations. Finally, the regions studied here offer a fairly large sample of young O and B-type stars suitable for spectral classification in the infrared, which will allow a much better characterization of the intrinsic properties of the stellar component of each HII region.

Acknowledgements. It is a pleasure to thank the staff of the Observatorio del Teide in Tenerife, and very especially to Dr. María Rosa Zapatero Osorio, for excellent support during the observations. The help of Ms. Petia Andreeva during the observing run and in the preparation of the figures presented in this paper is warmly acknowledged. Useful comments from the referee, Dr. S. Molinari, are also appreciated. This paper made extensive use of the SIMBAD Database maintained at the Centre de Données Stellaires in Strasbourg, France.

References

Altenhoff, W., Mezger, P. G., Wendker, H., & Westerhout, G. 1960, Veröff. Sternw. Bonn, 59, 48

Barsony, M., Scoville, N. Z., Bally, J., & Claussen, M. J. 1989, ApJ, 343, 212

Bessell, M., & Brett, J. M. 1988, PASP, 100, 1134

Bessell, M. S., Castelli, F., & Plez, B. 1998, A&A, 333, 231

Bochkarev, N. G., & Sitnik, T. G. 1985, ApSS, 108, 237

Bolton, J. G., & Westford, K. C. 1950, Aust. J. Sci. Res. A3, 251

Bronfman, L., Nyman, L.-Å, & May, J. 1996, A&AS, 115, 81

Campbell, M. F., Hoffmann, W. F., & Thronson, H. A. 1981, ApJ, 247, 530

Casali, M. M., & Hawarden, T. G. 1998, JCMT-UKIRT Newslett., 3, 33

Chan, S. J., Henning, Th., & Schreyer, K. 1996, A&AS, 115, 285

Churchwell, E., Walmsley, C. M., & Cesaroni, R. 1990, A&AS, 83, 119

Codella, C., Felli, M., & Natale, V. 1996, A&A, 311, 971

Cohen, R. J., Masheder, M. R. W., & Caswell, J. L. 1995, MNRAS, 274, 808

Comerón, F. 1997, A&A, 326, 1195.

Comerón, F., & Torra, J. 1999, A&A, 349, 605

Dent, W. R. F., MacDonald, G. H., & Andersson, M. 1988, MNRAS, 235, 1397

Dobashi, K., Bernard, J.-P., & Fukui, Y. 1996, ApJ, 466, 282

Dommanget, J. 1983, Bull. Inf. CDS, 24, 83

Downes, D., & Rinehart, R. 1968, ApJ, 144, 937

Elldér, J., Ronnang, B., & Winnberg, A. 1969, Nature, 222, 67

Elmegreen, B. G. 1998, in Origins, ASP Conf. Ser. 148

Garay, G., Rodríguez, L. F., Moran, J. M., & Churchwell, E. 1993, ApJ, 418, 368

Hodapp, K.-W., & Rayner, J. 1991, AJ, 102, 1108

Hofner, P., & Churchwell, E. 1996, A&AS, 120, 283

Jura, M., & Kleinmann, S. G. 1990, ApJS, 73, 769

Kleinmann, S. G., Sargent, D. G., Telesco, C. M., Joyce, R. R., & Gillett, F. C. 1979, ApJ, 227, 126

Knödlseder, J. 2000, A&A, 360, 539

Kurtz, S., Churchwell, E., & Wood, D. O. S. 1994, ApJS, 91, 659

Kurtz, S. E., Watson, A. M., Hofner, P., & Otte, B. 1999, ApJ, 514, 232

Kwok, S., Volk, K., & Bidelman, W. P. 1997, ApJS, 112, 557

Lockman, F. J. 1989, ApJS, 71, 469

Manchanda, R. K., Polcaro, V. F., Norci, L., et al. 1996, A&A, 305, 457

Mathys, G. 1987, A&AS, 71, 201

Mathys, G. 1989, A&AS, 81, 237

Matthews, H. E., Goss, W. M., Winnberg, A., & Habing, H. J. 1973, A&A, 29, 309

Matthews, N., Andresson, M., & Macdonald, G. H. 1986, A&A, 155, 99

Menten, K. M. 1991, ApJ, 380, L75

Molinari, S., Brand, J., Cesaroni, R., & Palla, F. 1996, A&A, 308, 573

Molinari, S., Brand, J., Cesaroni, R., Palla, F., & Palumbo, G. G. C. 1998, A&A, 336, 339

Odenwald, S. F. 1989, AJ, 97, 801

Odenwald, S., Shivanandan, K., Campbell, M., et al. 1986, ApJ, 306, 122

Odenwald, S. F., & Schwartz, P. R. 1989, ApJ, 345, L47

Odenwald, S. F., Campbell, M. F., Shivanandan, K., et al. 1990, AJ, 99, 288

Odenwald, S. F., & Schwartz, P. R. 1993, ApJ, 405, 706

Palla, F., Brand, J., Cesaroni, R., Comoretto, G., & Felli, M. 1991, A&A, 246, 249

Parthasarathy, M., Jain, S. K., & Bhatt, H. C. 1992, A&A, 266, 202

Piddington, J. H., & Minnett, H. C. 1952, Aust. J. Sci. Res. A5, 17

Piepenbrink, A., & Wendker, H. J. 1988, A&A, 191, 313

Pitault, A. 1981, A&A, 97, L5

Polcaro, V. F., & Norci, L. 1998, A&A, 339, 75

Polcaro, V. F., Giovannelli, F., Manchanda, R. K., Norci, L., & Rossi, C. 1991, A&A, 252, 590

Polcaro, V. F., Viotti, R., Rossi, C., & Norci, L. 1997, A&A, 325, 178

Price, S. D., Marcotte, L. P., & Murdock, T. L. 1982, AJ, 87, 131

Richards, P. J., Little, L. T., Toriseva, M., & Heaton, B. D. 1987, MNRAS, 228, 43

Rieke, G. H., & Lebofsky, M. J. 1985, ApJ, 288, 618

Roberts, D. A., Crutcher, R. M., & Troland, T. H. 1995, ApJ, 442, 208

Scalise, E., Rodríguez, L. F., & Mendoza-Torres, E. 1989, A&A, 221, 105

Schaerer, D., & de Koter, A. 1997, A&A, 322, 598

Shepherd, D. S., & Churchwell, E. 1996, ApJ, 457, 267

Shepherd, D. S., Churchwell, E., & Wilner, D. J. 1997, ApJ, 482, 355

Slysh, V. I., Val'tts, I. E., Kalenskii, S. V., et al. 1999, A&AS, 134, 115

Stetson, P. B. 1987, PASP, 99, 191

Szymczak, M., Hrynek, G., & Kus, A. J. 2000, A&AS, 143, 269

Tenorio-Tagle, G. 1979, A&A, 71, 59

Tokunaga, A. T. 2000, in Allen's Astrophysical Quantities, ed. A. N. Cox (AIP Press)

Turner, D. G., & Forbes, D. 1982, PASP, 94, 789

Watson, A. M., & Hanson, M. M. 1997, ApJ, 490, L165

Wendker, H. J. 1984, A&AS, 58, 291

Wendker, H. J., Higgs, L. A., & Landecker, T. L. 1991, A&A, 241, 551

Wink, J. E., Altenhoff, W. J., & Mezger, P. G. 1982, A&A, 108, 227